JOURNAL OF MATERIALS SCIENCE **40** (2005) 5941–5948

Numerical simulation of entangled materials mechanical properties

DAMIEN DURVILLE
LMSSMat, Ecole Centrale Paris/CNRS UMR 8579, Grande Voie des Vignes, 92295 Châtenay-Malabry Cedex, France
E-mail: durville@mssmat.ecp.fr

A general approach to simulate the mechanical behaviour of entangled materials submitted to large deformations is described in this paper. The main part of this approach is the automatic creation of contact elements, with appropriate constitutive laws, to take into account the interactions between fibres. The construction of these elements at each increment, is based on the determination of intermediate geometries in each region where two parts of beams are sufficiently close to be likely to enter into contact. Numerical tests simulating a 90% compression of nine randomly generated samples of entangled materials are given. They allow the identification of power laws to represent the evolutions of the compressive load and of the number of contacts.
© *2005 Springer Science + Business Media, Inc.*

1. Introduction

Entangled materials, which are made of fibres arranged together in various manners, usually exhibit a very specific and rather complex mechanical behaviour, characterized in particular by non linear loading curves. This complex behaviour originates from the contact-friction interactions which develop between fibres of such materials. Besides experimental studies, various analytical and numerical approaches have been suggested to explain and predict the mechanical behaviour of these materials. In correlation with measures on sheep wools, van Wyk [1] developed a model based on the estimation of the mean distance between contacts, and on the relation between the force and the deflection of a fibre between two contacts. Toll [2, 3] proposed a more complex theory, based in particular on the analysis of the structure tensors which characterize the morphology of the materials, and compared their results with experimental data obtained on polymer fibre masses. Baudequin *et al.* [4] derived a model from an analytical and statistical reasoning, which is in very good agreement with data issued from high compressive tests on glass wool. As far as numerical approaches are concerned, Beil and Roberts [5, 6] performed simulations for moderate compressions of fibre assemblies. Heyden [7] also used FE simulations in order to predict the failure of cellulose fibre networks.

We present here a general approach for the simulation of the mechanical behaviour of entangled materials, which has been designed for the consideration of large displacements and deformations. We consider samples of entangled materials as collections of fibres in which contact-friction interactions between fibres are taken into account as they occur. The specificity of our method lies in the detection of contacts between beams undergoing large displacements. Contact-friction interactions are taken into account at contact elements which couple two material particles. The main idea for the determination of these elements is the construction of intermediate geometries in all regions where parts of beams are close together and where contact is likely to appear. These intermediate geometries provide both with a geometric support for an a priori discretization of the contact problem, and with normal directions used for the contact search.

We present first the general setting of the problem together with the large displacements 3D-beam model used to represent the fibres, in order to write a principle of virtual works. Then, details are given about the way contact elements are created between the beams through the determination of intermediate geometries. The mechanical behaviour considered for these contact elements, in normal and tangential directions, is then formulated. The next section is devoted to the generation of the random samples used for the tests. Finally, we give numerical results for the simulation of a 90% compression applied to nine randomly generated samples of entangled materials with three different crimps. These results allow to identify the exponents of power laws to describe the evolutions of the compressive load and of the number of contacts.

2. Global problem setting

2.1. Beam model

We consider a collection of N fibres, described in a fictitious reference configuration by straight cylinders. The open set occupied in this configuration by the fibre

0022-2461 © *2005 Springer Science + Business Media, Inc.*
DOI: 10.1007/s10853-005-5061-2

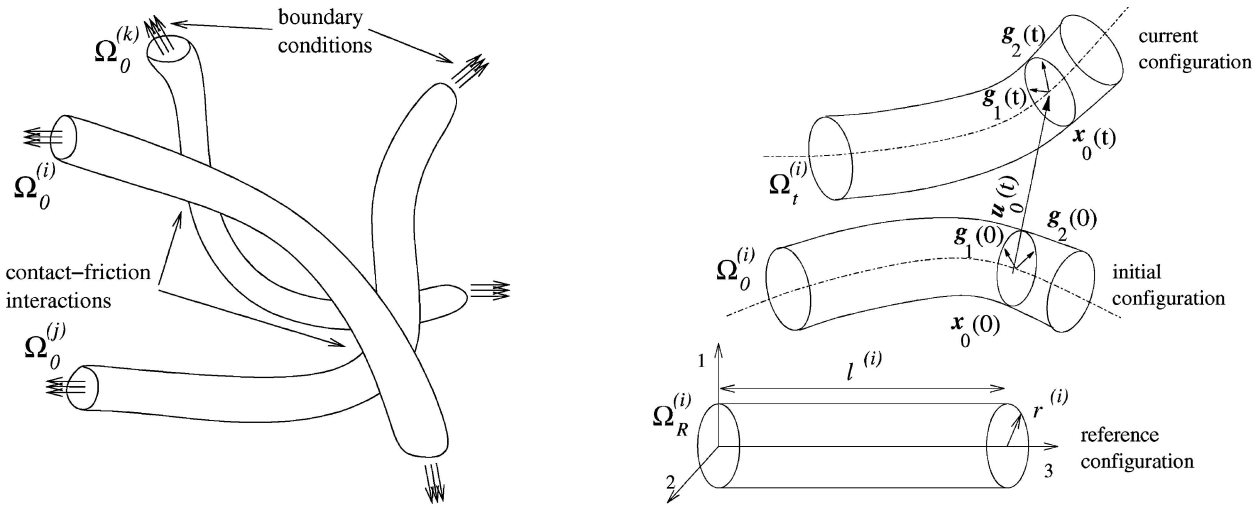

Figure 1 Setting of the global problem.

i, characterized by its radius $r^{(i)}$ and its length $l^{(i)}$, is denoted $\Omega_R^{(i)}$, and defined by:

$$\Omega_R^{(i)} = \left\{ \boldsymbol{\xi} = (\xi_1, \xi_2, \xi_3) \in \mathbb{R}^3; {\xi_1}^2 + {\xi_2}^2 \leq {r^{(i)}}^2, 0 < \xi_3 < L^{(i)} \right\}, \quad (1)$$

Each material particle $\boldsymbol{\xi}$ is identified in this configuration by its curvilinear abscissa ξ_3 and its coordinates (ξ_1, ξ_2) in the cross-section.

The kinematical beam model we use is characterized by the following expression of the placement of the particle $\boldsymbol{\xi}$ at time t:

$$\boldsymbol{x}(\boldsymbol{\xi}, t) = \boldsymbol{x}_0(\xi_3, t) + \xi_1 \boldsymbol{g}_1(\xi_3, t) + \xi_2 \boldsymbol{g}_1(\xi_3, t). \quad (2)$$

In this expression, $\boldsymbol{x}_0(\xi_3, t)$ is the placement of the centroid of the cross-section, and the two vectors $\boldsymbol{g}_1$ and $\boldsymbol{g}_2$ may be viewed as directors of the cross-section. This expression corresponds to a first order Taylor expansion of the placement with respect to sections coordinates. According to this model, the displacement of each particle, denoted $\boldsymbol{u}(\boldsymbol{\xi}, t)$, and defined by

$$\boldsymbol{u}(\boldsymbol{\xi}, t) = \boldsymbol{x}(\boldsymbol{\xi}, t) - \boldsymbol{x}(\boldsymbol{\xi}, 0), \quad (3)$$

can then be expressed

$$\boldsymbol{u}(\boldsymbol{\xi}, t) = \boldsymbol{u}_0(\xi_3, t) + \xi_1 \boldsymbol{h}_1(\xi_3, t) + \xi_2 \boldsymbol{h}_1(\xi_3, t). \quad (4)$$

The kinematics of each cross-section is thus described by the mean of three vectors: the translation $\boldsymbol{u}_0$ of the centroid, and two vectors $\boldsymbol{h}_1$ and $\boldsymbol{h}_2$ standing for the variations of the cross-section directors. This kinematical model is able to represent not only shear strain in the beam, but also planar deformations of the cross-sections. It allows in particular the use of classical 3D constitutive laws. In the following, we shall denote by $\boldsymbol{U}$ the generalized beam displacement field constituted by the three kinematical fields $\boldsymbol{u}_0$, $\boldsymbol{h}_1$ and $\boldsymbol{h}_1$:

$$\boldsymbol{U} = (\boldsymbol{u}_0, \boldsymbol{h}_1, \boldsymbol{h}_2). \quad (5)$$

2.2. Principle of virtual work

The global problem is set in the form of a principle of virtual work, which includes the virtual works of all beams of the collection, and the virtual work of contact-friction interactions between fibres. Defining for each beam a set of kinematically admissible generalized displacement fields $\mathcal{V}_{ad}^{(i)}$ satisfying the boundary conditions applied to its extremities, we express the global problem as follows:

Find $(\boldsymbol{U}^{(1)}, \ldots, \boldsymbol{U}^{(N)}) \in \mathcal{V}_{ad}^{(1)} \times \cdots \times \mathcal{V}_{ad}^{(N)}$, such that, $\forall (\boldsymbol{V}^{(1)}, \ldots, \boldsymbol{V}^{(N)}) \in \mathcal{V}_{ad}^{(1)} \times \cdots \times \mathcal{V}_{ad}^{(1)}$, we have:

$$\sum_{i=1}^{N} W_{int}^{(i)}\left(\boldsymbol{U}^{(i)}, \boldsymbol{V}^{(i)}\right) + W_{cf}\left(\boldsymbol{U}^{(1)}, \ldots, \boldsymbol{U}^{(N)}, \boldsymbol{V}^{(1)}, \ldots, \boldsymbol{V}^{(N)}\right) = 0. \quad (6)$$

In the above equation, the virtual work of internal forces for each fibre is expressed in the following way, using a total Lagragian formulation:

$$W_{int}^{(i)}(\boldsymbol{U}, \boldsymbol{V}) = \int_{\Omega_0^{(i)}} Tr\left(\boldsymbol{s}(\boldsymbol{U}) \frac{\boldsymbol{DE}}{\boldsymbol{DU}}.\boldsymbol{V}\right) d\boldsymbol{\omega} \quad (7)$$

where $\boldsymbol{U}$ is the generalized displacement field, $\boldsymbol{V}$, the corresponding virtual field, $\boldsymbol{E}$ is the Green-Lagrange strain tensor and $\boldsymbol{s}$ the second Piola-Kirchhoff stress tensor.

The purpose of the next sections is the expression of the virtual work of contact-friction interactions W_{cf}.

3. Detection of contacts within a collection of fibres

The detection of contacts between fibres is one of the main difficulties of the problem. In the media considered here, since the geometry and the arrangement of fibres evolve continuously, contact may appear or disappear anywhere, and at any time, and the number of contacts increases as the medium is densified.

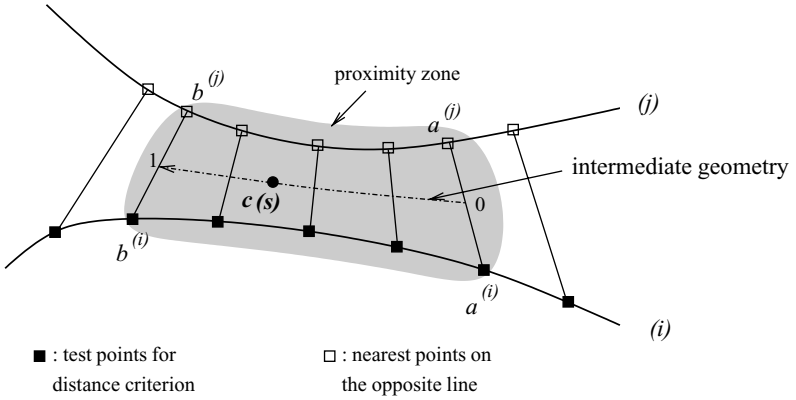

Figure 2 Proximity zone and intermediate geometry.

3.1. General presentation of the method

The method we suggest to treat the contact in such media, and which will be developed below, is based on an a priori discretization of the contact problem, defined on intermediate geometries that are constructed in all regions where two parts of fibres are close together. This approach is motivated by the following reasons. First, as far as the discretization is concerned, within a continuous framework, contact would be defined as two parts of surfaces of fibres having coincident positions. However, interpolated surfaces, such as that encountered in meshes, can not adjust exactly to each other in the general case, and consequently, contact conditions between these surfaces can only be checked at some discrete points. Starting from this point, we choose to set the contact problem in a discretized way, that is to check contact between fibres only at some discrete points that will be defined depending only on geometrical criteria.

The second point, which is also related to the discretization, is that contact interactions between fibres, especially at crossings between them, are localized at very precise places, that do not necessarily coincide with nodes or other particular points of the meshes. This means that the contact detection must be independent on the positions of the nodes.

The last motivation for our method deals with the question of the contact search direction used to associate points of the structure that are predicted to enter into contact. Usually, in classical methods, the normal direction to one surface is used to search a contact on the opposite surface. This choice may reveal not suitable for structures with high curvatures, where the normal directions have large variations. Moreover, it leads to a treatment which is non symmetrical with respect to the two opposite geometries. To improve the choice of the contact search direction, it seems desirable to make this direction depend on both opposite geometries. A good way to achieve this is to consider the geometry corresponding to the average of the potentially contacting surfaces, and to take the normal direction to this intermediate geometry as the contact search direction.

For the case of beams, this intermediate geometry reduces to a part of line, defined as the average of two portions of lines of centroids of beams which are declared to be close to each other. The normal directions to this geometry are given by planes orthogonal to this line.

3.2. Determination of proximity zones and intermediate geometries

We define proximity zones as parts of lines of centroids of beams which are close to each other. To determine them, for each pair of fibres in the collection, we calculate the distances between points regularly distributed on one of the lines of centroids, and their corresponding closest point on the other line. The intervals of curvilinear abscissa delimited by successive pairs of close points define a pair of close parts of lines (see Fig. 2). Some corrections may be necessary in order these two parts of line are oriented in the same direction, have a minimal length and are nearly centered on the minimal distance between them. At the end of this process, we obtain a set of proximity zones, denoted $\mathcal{P}_m$, and defined by

$$\mathcal{P}_m = \left[a^{(i)}, b^{(i)}\right] \times \left[a^{(j)}, b^{(j)}\right], \tag{8}$$

where $[a^{(i)}, b^{(i)}]$ and $[a^{(j)}, b^{(j)}]$ are two intervals of curvilinear abscissa defined on beams i and j.

The intermediate geometry Γ_{int} associated with this proximity zone is defined as the average of the close parts of line. The position of any point $\boldsymbol{c}$ on this geometry, at the relative abscissa s, is defined by

$$\begin{aligned}\boldsymbol{c}(s) = \frac{1}{2}\big[&\boldsymbol{x}_0^{(i)}\big((1-s)a^{(i)} + sb^{(i)}\big) \\ &+ \boldsymbol{x}_0^{(j)}\big((1-s)a^{(j)} + sb^{(j)}\big)\big]\end{aligned} \tag{9}$$

The tangent to the intermediate geometry at the relative abscissa s, $\boldsymbol{T}_c(s)$, is obtained by derivating the above expression.

3.3. Construction of contact elements on intermediate geometries

The discretization of the contact problem is obtained by distributing on the intermediate geometry a given number N_c of points where the contact has to be checked. Each contact checking point, denoted $\boldsymbol{c}_k$, is defined by

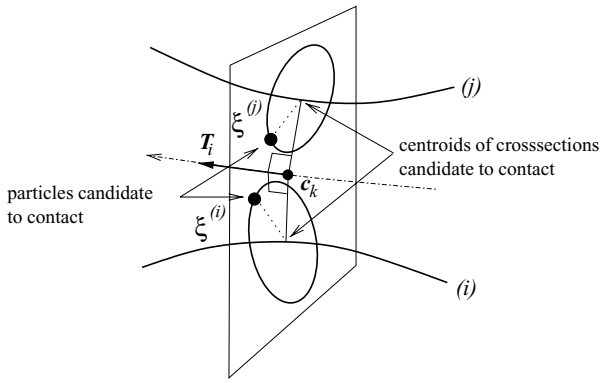

Figure 3 Determination of the particles of a contact element.

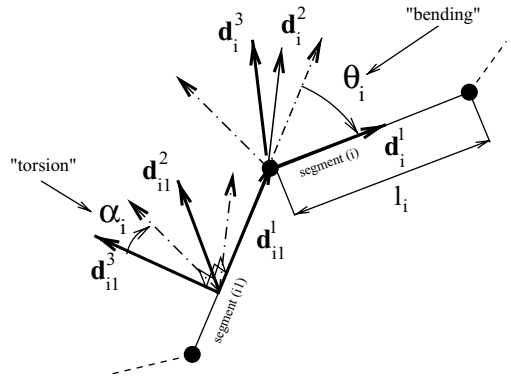

Figure 4 Generation of random segments.

its relative abscissa $s_k = (k-1)/(N_c - 1)$ on the intermediate geometry.

In the equilibrium configuration, the contact element at the point $\boldsymbol{c}_k$, denoted $E_c(\boldsymbol{c}_k)$ would be defined as the couple of material particles localized at this point:

$$E_c(\boldsymbol{c}_k) = \left(\boldsymbol{\xi}^{(i)}, \boldsymbol{\xi}^{(j)}\right) \in \Omega_R^{(i)} \times \Omega_R^{(j)}, \text{ such that}$$
$$\boldsymbol{x}^{(i)}\left(\boldsymbol{\xi}^{(i)}\right) = \boldsymbol{x}^{(j)}\left(\boldsymbol{\xi}^{(j)}\right) = \boldsymbol{c}_k. \tag{10}$$

However, for the out-of-equilibrium configurations we have to deal with during the iterations of the non linear algorithm, contact conditions are generally not satisfied. In this case, the particles constituting the contact elements can no longer be characterized by their identical positions ; they can only be determined through predictions. To predict which particles will enter into contact at a given point of the intermediate geometry, we proceed in the following way. First, the centroids cross-sections candidate to contact are located at the intersections with the normal plane to the intermediate geometry at $\boldsymbol{c}_k$ (see Fig. 3). Then, in a second step, the particles of the contact element are chosen on the border of these cross-sections, using the projection on each cross-section of the direction between the two centroids.

3.4. Determination of the contact normal direction

The contact normal direction is used in the expressions of the normal gap and of the tangential relative displacement used to determine contact-friction interactions. The determination of this unit vector, whose part is to give the direction of contact, is of great importance to prevent the fibres to go across each other. A good choice for this direction is to take, near the crossing between fibres, the vector product between the tangents to the lines of centroids. At a certain distance from crossings, or when fibres are almost parallel, it is possible to take for this vector the direction between the centroids of cross-sections in interaction. If we denote $\boldsymbol{N}$ this contact normal direction, the linearized contact condition for the contact element $E_c(\boldsymbol{c}_k)$ may be expressed as follows:

$$gap(E_c(\boldsymbol{c}_k)) = \left(\boldsymbol{x}^{(i)}\left(\boldsymbol{\xi}^{(i)}\right) - \boldsymbol{x}^{(j)}\left(\boldsymbol{\xi}^{(j)}\right), \boldsymbol{N}(E_c(\boldsymbol{c}_k))\right) \geq 0. \tag{11}$$

As far as the tangential part is concerned, we use the same vector to define the tangential relative displacement $[\boldsymbol{U}]_T(E_c(\boldsymbol{c}_k))$:

$$[\boldsymbol{U}]_T(E_c(\boldsymbol{c}_k)) = [\boldsymbol{I} - \boldsymbol{N}(E_c(\boldsymbol{c}_k)) \otimes \boldsymbol{N}(E_c(\boldsymbol{c}_k))] \times \left(\boldsymbol{U}^{(i)}\left(\boldsymbol{\xi}^{(i)}\right) - \boldsymbol{U}^{(j)}\left(\boldsymbol{\xi}^{(j)}\right)\right). \tag{12}$$

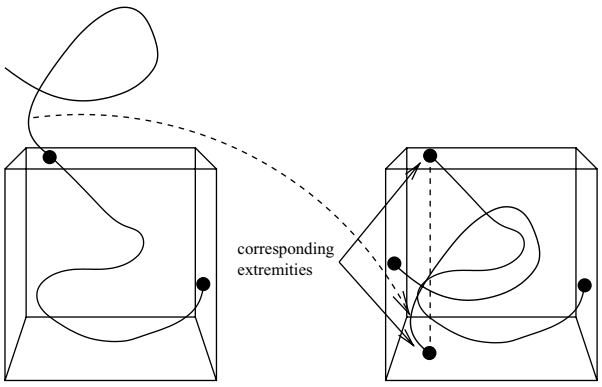

Figure 5 Cutting of the random line to have corresponding extremities between fibres.

4. Virtual work of contact-friction interactions

The virtual work of contact-friction interactions for the contact element $E_c(\boldsymbol{c}_k)$ is expressed in the following way

$$W_{cf}(E_c(\boldsymbol{c}_k)) = (R_N(gap(E_c(\boldsymbol{c}_k)))\boldsymbol{N} + \boldsymbol{R}_T([\boldsymbol{U}]_T(E_c(\boldsymbol{c}_k))), \boldsymbol{V}^{(i)}\left(\boldsymbol{\xi}^{(i)}\right) - \boldsymbol{V}^{(j)}\left(\boldsymbol{\xi}^{(j)}\right) \tag{13}$$

where R_N is the norm of the normal reaction, and $\boldsymbol{R}_T$ the tangential frictional reaction.

As far as the normal behaviour is concerned, the normal reaction R_N is expressed in function of the gap using a regularized penalty method:

$$\text{if } gap \geq 0; \quad R_N(gap) = 0, \tag{14}$$

$$\text{if } g_r \leq gap < 0; \quad R_N(gap) = \frac{k_N}{2g_r} gap^2, \tag{15}$$

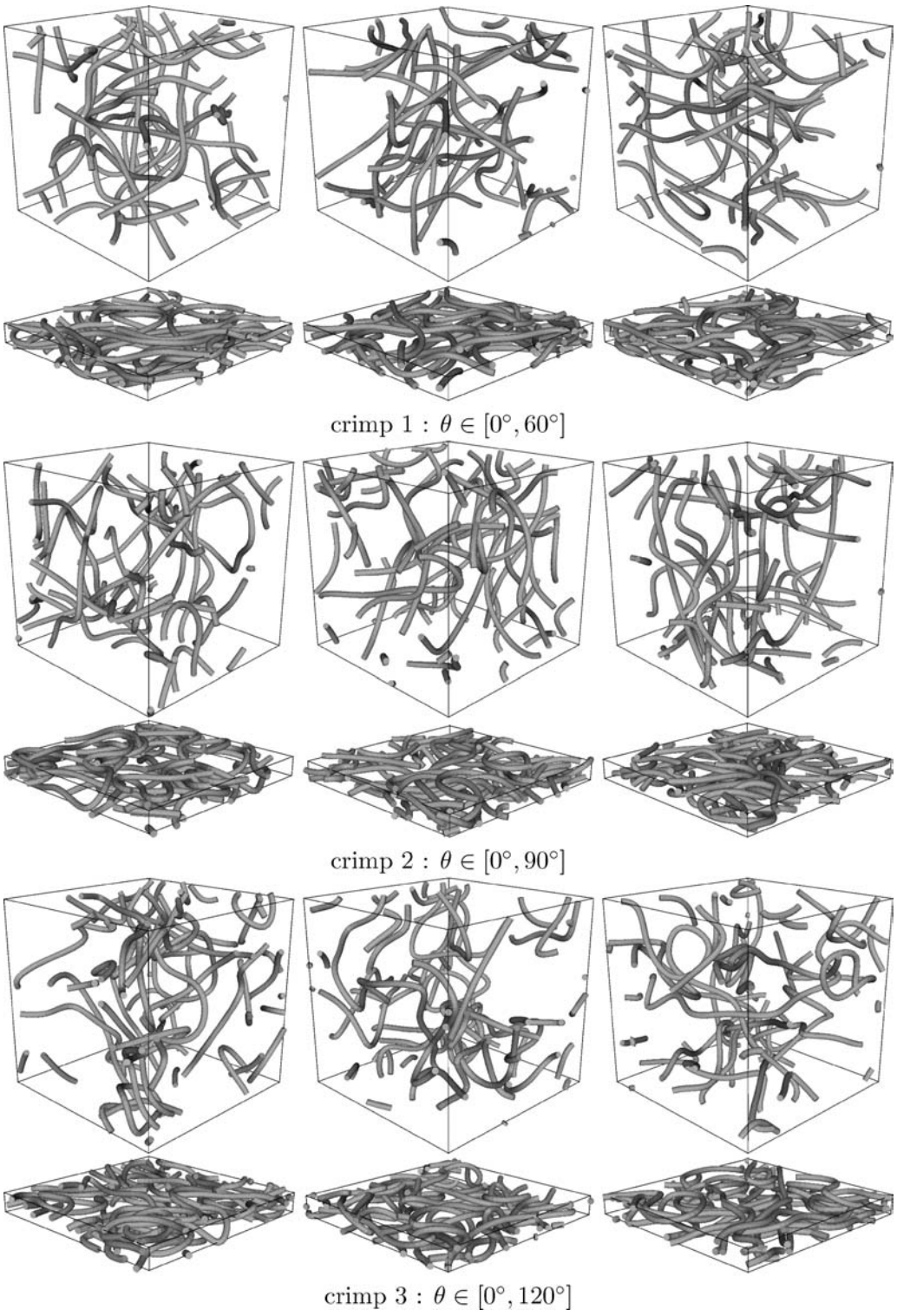

Figure 6 Initial and final configurations of the nine samples for the three different crimps.

$$\text{if } gap < g_r; \quad R_N(gap) = k_N \left(gap + \frac{g_r}{2} \right). \quad (16)$$

In this expression, k_N is the penalty coefficient, and g_r the regularization threshhold. This regularization, for very small penetrations, makes the reaction depend quadratically on the gap, which ensures the continuity of its derivate at the origin.

For the tangential components, we use a regularized Coulomb's law, which allows a small reversible displacement before the pure sliding occurs. The tangential reaction is expressed as follows as function of the tangential relative displacement:

$$\text{if} [\boldsymbol{U}]_T(E_c(\boldsymbol{c}_k)) \leq u_{T,\text{rev}}, \quad \boldsymbol{R}_T(E_c(\boldsymbol{c}_k)) = \frac{\mu \|\boldsymbol{R}_N\|}{u_{T,\text{rev}}} [\boldsymbol{U}]_T(E_c(\boldsymbol{c}_k)) \quad (17)$$

$$\text{else } \boldsymbol{R}_T(E_c(\boldsymbol{c}_k)) = \frac{\mu \|\boldsymbol{R}_N\|}{\|[\boldsymbol{U}]_T\|} [\boldsymbol{U}]_T(E_c(\boldsymbol{c}_k)) \quad (18)$$

where μ denotes the Coulomb's friction coefficient, and $u_{T,\text{rev}}$ is the reversible tangential displacement.

Adaptation of the penalty coefficient. In order to stabilize the algorithm, the penalty coefficient is adapted, for each proximity zone, in such a way that the maximum penetration among all contact elements of this zone remains inferior to a given value. This is very useful since resultant reactions may vary largely from one zone to another, and during the loading.

5. Generation of random periodic samples for the simulation

The generation of the samples for the simulation must fulfill two requirements: the random geometries of the fibres have to satisfy some criteria such as the crimp and the structure of these samples must be adapted to the application of periodic boundary conditions.

5.1. Generation of random lines

The geometries of the fibres are parts of a global random line. To build this line, as a first step, a series of straight segments is generated. Each of these segment is characterized by its length l_i, and two angles, α_i and θ_i which may be viewed as a torsion angle and a a bending angle with respect to the previous segment (see Fig. 4). To create the line, the three parameters of these segments are randomly taken in given intervals of variation. To obtain different crimps, we keep the intervals of variation for the length and the torsion angle constant, but make the interval for the bending angle θ vary. Finally, to get a line with a C2 regularity, this series of points is smoothed by the means of B-splines.

5.2. Adaptation to the application of periodic boundary conditions

A good way to facilitate the application of periodic conditions on samples of entangled materials is to have correspondances between extremities of fibres on opposite faces of the sample. To achieve this, having defined the box that will contain the sample to be created, we start by placing the random line at one point on a face of the sample. Then, the line is cut each time it goes through a face, and the remaining of the line is placed at the same position on the opposite face (see Fig. 5). In this way, except for the first and last extremities, each extremity of a fibre has a corresponding extremity on the opposite face, at the same relative location, and with the same orientation with respect to the face.

6. Numerical results

6.1. Objectives

To illustrate the performances of the methodology presented here, tests have been run on nine randomly generated samples of entangled media. Through these tests, we aim at identifying constitutive laws for the compressive behaviour of such materials, while studying the influence of the crimp on the results.

6.2. Characteristics of the samples

For the tests, we have taken arbitrary fixed values for the mechanical characteristics. Geometrical characteristics, which are more important regarding the results, are summarized in Table I. To obtain different crimps, we have taken three ampltiudes of variation, 60°, 90° and 120°, for the bending angle θ introduced in the

TABLE I Geometrical characteristics of samples

Sample size	$1 \times 1 \times 1$
Fibres radius	0.015
Initial volume fraction	2%
Number of fibres per sample	≈ 50

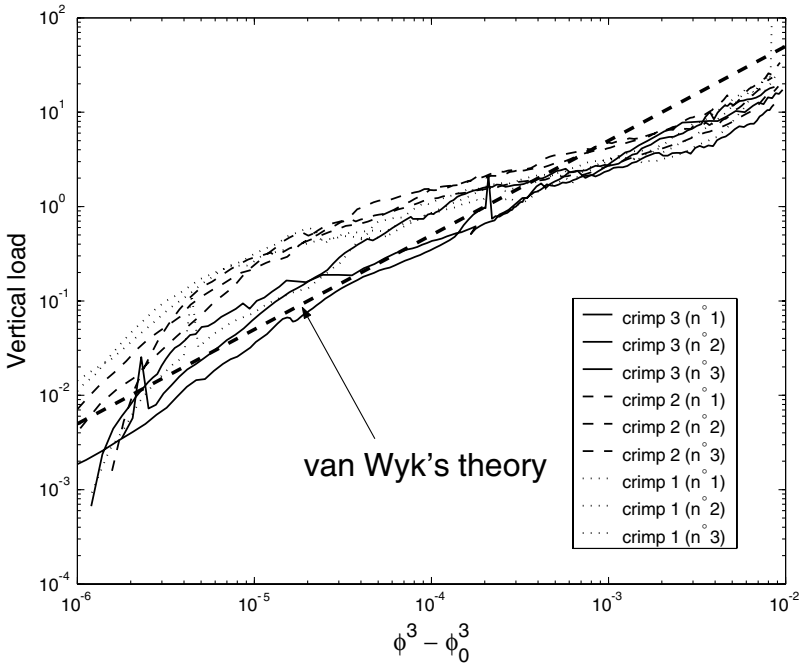

Figure 7 Comparison of loading curves with van Wyk's theory.

generation of the basic random line (see Section 5.1). Three random samples have been generated for each crimp. The samples comprise about 50 fibres, and a friction coefficient of 0.2 has been considered.

6.3. Discussion about the results

The nine samples have been submitted to a 90 % compression (Fig. 6). Loading curves for each sample present some irregularities and instabilities, but they behave globally in the same way. In order to identify constitutive laws we have plotted the variations of the compressive load versus different quantities. According to van Wyk's model [1], this load is proportional to $\phi^3 - \phi_0^3$, where ϕ and ϕ_0 are respectively the initial and the current volume fraction of fibres. The curves on Fig. 7 show a better agreement with this model as the crimp is higher.

We found a better correlation between the loading curve and the relative variation of the volume fraction, namely $(\phi - \phi_0)/\phi_0$. The results plotted on Fig. 8 tend to indicate that, until 85% of compression, the vertical load F follows the law

$$F \propto \left(\frac{\phi - \phi_0}{\phi_0}\right)^{\frac{3}{2}}. \tag{19}$$

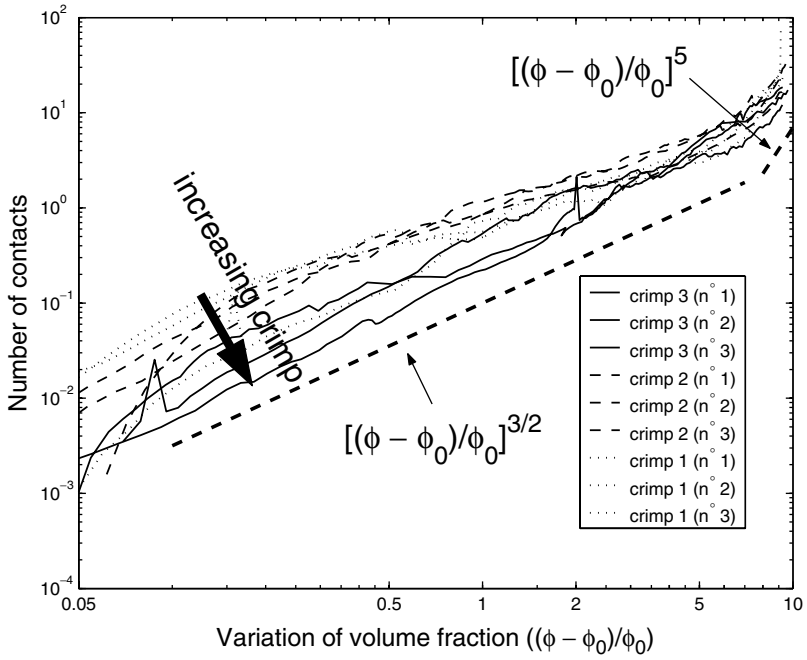

Figure 8 Evolutions of the compressive load versus the relative variation of volume fraction.

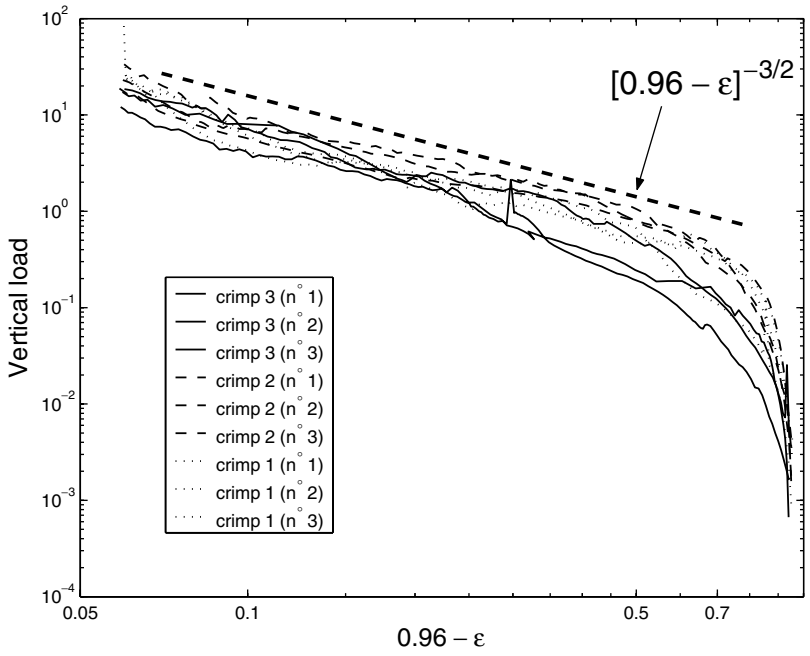

Figure 9 Fitting of the loading curves for high compressions.

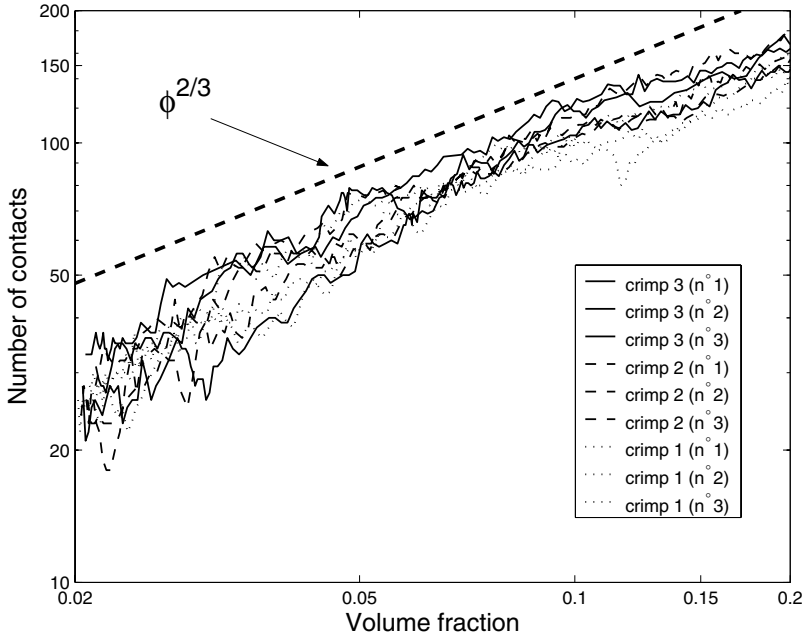

Figure 10 Comparison between the evolutions of numbers of contacts versus volume fraction.

Here again, we obtain a better fitting with this expression as the crimp is higher. For larger compressions, the exponent of the power law increases up to 5.

Baudequin *et al*. [4] studied more precisely the behaviour of samples of glass wool at high compressions. From their analytical model and their experimental data, they derived the following expression of the vertical load

$$F \propto \left(\epsilon^\star - \epsilon\right)^{-\frac{3}{2}} \tag{20}$$

where ε is the compressive deformation and $\epsilon^\star$ is the maximum compressive strain, which they estimate to be equal to 0.96. Plotting the variation of the vertical load versus $\epsilon^\star - \epsilon$ (see Fig. 9), our numerical results appear also in good agreement with this prediction. This should have been expected as formulae (19) and (20) are very close as $\epsilon^\star$ goes to 1.

Finally, the curves describing the evolution of the number of contacts during the loading (Fig. 10) show that this number, denoted n_{ct}, is proportional to the volume fraction of fibres to the power 2/3:

$$n_{ct} \propto \phi^{\frac{2}{3}} \tag{21}$$

7. Conclusion

Our approach to take into account contact-friction interactions within a collection of 3D beams, based on the determination of intermediate geometries to generate automatically contact elements, has proven its ability to simulate the mechanical behaviour of general entangled materials submitted to large transformations. The results of the tests performed on nine random samples allow the identification of exponents of power laws to represent the evolutions of the compressive load and of the number of contacts. In particular, it has been shown that for these cases, and for moderate compressions, the compressive load evolves as the relative variation of volume fraction to the power 3/2.

References

1. T. W. MCDEVITT and T. A. LAURSEN, *Intern. J. Numer. Meth. Engng.* **48** (2000) 1525.
2. D. DURVILLE, Modélisation du comportement mćanique des câbles métalliques, *Revue Européenne des Éléments Finis* **7**(1–3) (1998) 9.
3. G. ZAVARISE and P. WRIGGERS, *Intern. J. Numer. Meth. Engng.* **49** (2000) 977.
4. M. BAUDEQUIN, G. RYSCHENKOW and S. ROUX, *The European Physical J. B* **12** (1999) 157.
5. C. M. VAN WYK, *J. Textile Inst.* **37** (1946) 285.
6. S. TOLL and J.-A. E. MANSON, *J. Appl. Mech.-T. ASME* **38** (1995) 223.
7. S. TOLL, *Polymer Eng. Sci.* **38** (1998) 1337.
8. N. B. BEIL and W. W. ROBERTS, JR., *Textile Res. J.* **72**(4) (2002) 341.
9. N. B. BEIL and W. W. ROBERTS, JR., *Textile Res. J.* **72**(5) (2002) 375.
10. S. HEYDEN, Network modelling for the evaluation of mechanical properties of cellulose fibre fluff, Lund University, Sweden (2000).

Received December 2004
and accepted April 2005